A&A 423, 613–628 (2004)
DOI: 10.1051/0004-6361:20040566

Astronomy & Astrophysics

Doppler imaging of stellar non-radial pulsations

I. Techniques and numerical experiments

O. Kochukhov

Institut für Astronomie, Universität Wien, Türkenschanzstraße 17, 1180 Wien, Austria
e-mail: oleg@astro.univie.ac.at

Received 31 March 2004 / Accepted 29 April 2004

Abstract. We present a novel technique aimed at the investigation of the geometry of surface velocity fluctuations in non-radially pulsating stars. Our method is based on the Doppler imaging principle and enables an accurate reconstruction of a two-dimensional map of the pulsational disturbances using spectroscopic time-series observations. No specific assumptions on the shape of the pulsation geometry are made. This opens a unique possibility to go beyond the traditional mode identification analyses and study complex rotationally and magnetically distorted non-radial pulsation modes which cannot be described by a single spherical harmonic function. Performance and intrinsic limitations of the new Doppler imaging procedure are assessed with inversions of simulated data. Based on the results of these numerical tests we conclude that a reliable recovery of the surface pulsation velocity structures can be achieved for all types of pulsation geometries accompanied by significant line profile variations. It is also demonstrated that the Doppler mapping of the pulsation velocity field is remarkably robust with respect to errors in the adopted stellar parameters.

Key words. stars: oscillations – stars: imaging – line: profiles

1. Introduction

1.1. Identification of pulsation modes

Many types of stars across the Hertzsprung-Russell diagram are found to pulsate in non-radial modes. Pulsational parameters determining periodic oscillations of the stellar brightness and pulsational changes in the absorption line profiles observed at high time and spectral resolution contain unique information about fundamental characteristics and internal structure of stars. Consequently, detailed observations and interpretation of stellar pulsational fluctuations is a powerful tool to probe underneath the thin outer stellar layers accessible to direct observations and, eventually, to verify and constrain theoretical models of stellar structure and evolution via the asteroseismological analysis. To enable a meaningful comparison of the instabilities appearing in the theoretical stellar oscillations models and the observed pulsation frequencies it is necessary to identify pulsation modes. In the idealized case of a simple non-radial oscillation described by a single spherical harmonic function the mode identification procedure reduces to assigning a degree ℓ and azimuthal number m to the observed pulsation frequencies. This problem is solved by several spectroscopic mode identification techniques (see recent reviews by Aerts & Eyer 2000; Balona 2000; Telting 2003). With the best observational data these methods are typically able to estimate ℓ and $|m|$ values with an accuracy of ± 1.

In a broader context of rotating magnetized stars the approximation of non-radial pulsations with a single spherical harmonic becomes invalid. Even a relatively slow rotation induces important toroidal terms in the description of the surface pulsation geometry (Martens & Smeyers 1982; Aerts & Waelkens 1993). In rapidly rotating stars situation becomes considerably more complicated: the series of spherical harmonics required for an accurate description of pulsational perturbations has to include contributions of many components characterized by the same m but different ℓ values (e.g. Lee & Saio 1990).

An even more challenging situation is encountered by the studies of p-mode pulsations in magnetic chemically peculiar (roAp) stars, whose equilibrium structure deviates from axisymmetry. These middle main sequence stars are thought to pulsate in high-overtone, low-degree ($\ell \lesssim 3$) modes aligned with an oblique quasi-dipolar stellar magnetic field rather than with the stellar axis of rotation (Kurtz 1982). In addition to constraining an orientation of the pulsation axis, the magnetic effects are coupled with the slow rotation of roAp stars and are expected to significantly distort a simple oblique axisymmetric shape of the roAp pulsations (Shibahashi & Takata 1993; Bigot & Dziembowski 2002; Saio & Gautschy 2004) leading to a representation of oscillations by a sum of terms with different ℓ and m values, which results in further complications for the traditional mode identification techniques. Up to now no satisfactory solution for an accurate reconstruction of the

geometry of rotationally and magnetically distorted non-radial modes has ever been found. The only known approach that can, in principle, be applied to study distorted modes, is subjective and time-consuming direct trial-and-error spectrum synthesis fitting of the observed stellar line profile shapes (Smith 1977).

1.2. Doppler imaging and its application to non-radial pulsations

It has been understood that reconstruction of the stellar surface structures can be dramatically improved by utilizing a resolution of the stellar surface provided by the stellar rotation. If the projected rotational velocity of a star is large enough for the shapes of spectral lines to be dominated by the rotational Doppler broadening (in practice, $v_{\rm e} \sin i \gtrsim 20$ km s^{-1} is required), there exists a well-defined mapping relation between distortions in a line profile and positions of inhomogeneities on the stellar surface. The Doppler-broadened line profile represents a one-dimensional projection of the stellar surface, with all the structure blurred along the lines of constant Doppler shift. Spectroscopic observations at different rotation phases can be used to monitor the evolution of dips and bumps in line profiles, thus obtaining a set of non-redundant projections of a stellar surface map, and eventually reconstruct a two-dimensional image from a time series of line profile observations. This Doppler imaging (DI) method was first applied by Goncharskii et al. (1977) to the problem of mapping surface chemical inhomogeneities in Ap stars and was subsequently extended to mapping temperature spots (Vogt et al. 1987) and magnetic fields (Brown et al. 1991) in active late-type stars.

Recently Piskunov & Kochukhov (2002) and Kochukhov & Piskunov (2002) have generalized the Doppler imaging technique to modelling rotational variability of the stellar spectra in all four Stokes parameters and carried out simultaneous mapping of vector magnetic fields and abundance inhomogeneities in chemically peculiar stars. These investigations demonstrated that DI is successful even when a mapping relation between the wavelength position inside a line profile and position on the stellar surface is not known in advance but is described by a complex function of the local parameters, such as magnetic field strength and orientation.

The rotational Doppler broadening of stellar line profiles can also be successfully used to probe the horizontal structure of non-radial pulsations. Vogt & Penrod (1983) were the first to demonstrate how rapid rotation enhances the visibility of profile distortions due to high-order pulsation modes and opens new prospects for mode identification. A series of subsequent investigations presented several modifications of the mode identification technique utilizing the effect of partial Doppler resolution of the stellar surface (Gies & Kullavanijaya 1988; Kennelly et al. 1992; Hao 1998). In all these approaches pulsation velocity field is parameterized with a single spherical harmonic function. The respective mode identification analysis does not require detailed line profile modelling but typically uses a number of restrictive assumptions, for instance, that the star is seen equator-on and/or pulsation modes are described by the sectoral ($\ell = |m|$) spherical harmonics only. Although these techniques are often collectively referred to as "Doppler imaging", they use only part of the information contained in stellar line profiles, namely the resolution of the velocity structures along the stellar longitudes. Unlike in classical Doppler imaging inversions, widely applied nowadays to mapping spots in magnetic Ap and late-type active stars, the possibility of obtaining latitudinal resolution by observing surface structures from varying aspect remained unexplored in the analyses of non-radially pulsating stars.

In this paper we present the first attempt to extend the principles of Doppler imaging inversion technique to the problem of reconstruction of the stellar pulsation velocity field. We suggest that the horizontal pulsation pattern can be recovered through a detailed modelling of the pulsational changes of line profile shapes *and* modulation of this variability by the stellar rotation. The main novelty of the suggested technique is that i) reconstruction of the stellar velocity map is carried out without assuming that pulsations have a presupposed shape and ii) we fully exploit the information provided by the changes of aspect at which the pulsation geometry is observed as a result of the stellar rotation.

The following sections describe the basic assumptions and numerical techniques implemented in the new pulsational Doppler imaging code. Capabilities and intrinsic limitations of the proposed mapping method are assessed using inversions of simulated observational data for different pulsation modes.

Our pulsational Doppler imaging code is sufficiently general to be applied to all types of non-radial pulsators. However, at the moment we mainly focus on oblique pulsations in roAp stars, which obviously present the best prospects for pulsational Doppler mapping due to an extraordinary rotational modulation of the observed pulsation characteristics.

1.3. Velocity vs. temperature pulsational mapping

In a recent study Berdyugina et al. (2003, hereafter referred to as BTK) presented a somewhat similar exploration of the capabilities of the Doppler imaging technique in its application to mapping of stellar non-radial pulsations. These authors assumed that pulsational fluctuations at the stellar surface can be represented by a rotation of a fixed pattern and used a regular *temperature* Doppler imaging code to model pulsational line profile variations.

In our opinion some of the approximations intrinsic to the method of BTK preclude reliable reconstruction of the pulsation geometry and make impossible wide application of this technique to the problem of imaging the surface structure of stellar non-radial pulsations. First, the key assumption that non-radial pulsations can be described by a pattern-rotation fails for many astrophysically interesting situations where the pulsation geometry cannot be reduced to a pattern aligned with the stellar rotation axis and characterized by a single non-zero m value. This means that the method of BTK is not applicable to a study of axisymmetric non-radial modes in normal pulsators or oblique p-mode pulsations in roAp stars. Furthermore, the pattern-rotation description actually supposes that a good guess of pulsation mode identification is available prior to the

Doppler analysis because the required input pattern-rotation period is itself derived from the observed pulsation frequency *and* the absolute value and the sign of the azimuthal number m of a pulsation mode. Thus, contrary to the claim made by BTK that their method is free from the spherical harmonic parameterization of non-radial pulsations, they implicitly used a rather restrictive assumption about the surface geometry of pulsational disturbances. For their method to work, pulsations have to be described by a combination of spherical harmonics, which is aligned with the stellar axis of rotation and has a predetermined non-zero and unique azimuthal number m.

Secondly, the description of line profile variations with only temperature fluctuations is inadequate for the vast majority of non-radially pulsating stars. The line profile changes during oscillation cycle are mostly determined by the pulsation velocity field, while the corresponding temperature variations have hardly any influence at all (De Ridder et al. 2002). In addition to this fundamental physical background, the Doppler mapping of temperature and velocity are characterized by markedly different relations between structures in the observed line profiles and location of the surface inhomogeneities. This is illustrated in Fig. 1, which shows the temperature map required to approximately reproduce the spectral line profile computed for a specific phase of the $\ell = 6$, $m = 6$ non-radial pulsations. We note that the match between profile distortions produced by the velocity fluctuations and the temperature map is not exact: the line profile corresponding to the former type of surface distribution tend to have narrower dips and broader bumps. Furthermore, in the case of non-radial velocity fluctuations, bumps and dips in line profiles are produced by redistribution of the line absorption due to a complex surface pattern of projected Doppler shifts affecting radiation coming from different surface zones. On the other hand, in the presence of temperature inhomogeneities, the line profile distortions are produced by the genuine lack or excess of absorption, mainly resulting from different continuum brightness of the regions located on the visible stellar hemisphere. In this case the mapping between the wavelength position in a line profile and position across the stellar disk occurs strictly along the vertical stripes of constant rotational Doppler shift, while this is not true for the surface velocity fluctuations. This crucial difference between the temperature and velocity surface mapping indicates that, in general, the two types of surface distortions cannot be interchanged without introducing severe artifacts in the reconstructed Doppler maps. This suggests that the temperature mapping of velocity pulsations can work satisfactorily only in exceptional situations where a non-radial mode has an especially simple pattern of a superposition of the rotational and pulsational Doppler shifts, as it happens, for instance, for the sectoral, $\ell = |m|$, pulsations observed at high inclination angles.

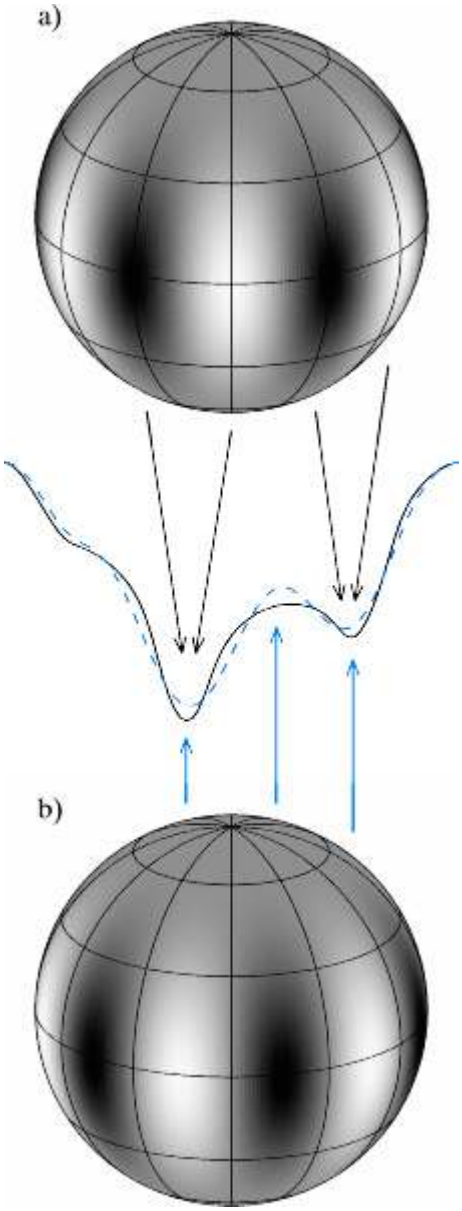

Fig. 1. Illustration of the mapping between position across the stellar disk and distortions in the spectral line profiles of a rapidly rotating star. The vertical component of the surface velocity field due to the $\ell = 6$, $m = 6$ non-radial pulsation mode (a), solid line) is compared with a temperature distribution (b), dashed line) required to roughly reproduce the pulsational line profile distortions (middle panel). The darker areas in the velocity image show surface zones receding from the observer, while the lighter areas correspond to material moving towards the observer. In the temperature map brighter regions correspond to higher local temperature.

In contrast to the approach proposed by BTK, in this paper we describe a Doppler mapping technique that does not need any direct or indirect a priori assumptions about geometry of the surface pulsational fluctuations. With our method the line profile variations are modelled using physically realistic description of pulsations with a time-dependent velocity field. These features of the proposed Doppler imaging method allow us to study pulsation modes of an arbitrary complexity. Furthermore, in mapping non-radial velocity field we are also able to take into account the presence of surface chemical abundance inhomogeneities, which are relevant for some types of middle and upper main sequence pulsators and can introduce additional important modulation of the line profile shapes and strengths.

2. Velocity field due to non-radial oscillations

Our description of the stellar pulsation velocity field generally follows that of Schrijvers et al. (1997). In the limit of no rotation solution of the basic perturbation problem for a monoperiodic pulsator leads to the following form of the Lagrangian displacement vector in spherical coordinates

$$\boldsymbol{\xi} = \sigma_r \left\{1, K\frac{\partial}{\partial\theta}, K\frac{1}{\sin\theta}\frac{\partial}{\partial\phi}\right\} N_\ell^m Y_\ell^m(\theta,\phi)\,\mathrm{e}^{\mathrm{i}\omega t+\chi_0}, \quad (1)$$

where the ratio of the horizontal σ_t and vertical σ_r pulsation amplitude can be estimated according to the outer mechanical boundary condition

$$K \equiv \frac{\sigma_t}{\sigma_r} = \frac{GM}{\omega^2 R^3} \quad (2)$$

(e.g. Smeyers & Tassoul 1987). Here R and M are the stellar mass and radius, ω is the angular pulsation frequency and G represents the gravitational constant. Parameter χ_0 in the exponent of Eq. (1) corresponds to a fixed phase constant. The spherical harmonics $Y_\ell^m(\theta,\phi)$ determining the geometry of pulsational perturbations are functions of the stellar latitude θ and azimuth ϕ and are given by

$$Y_\ell^m(\theta,\phi) \equiv P_\ell^{|m|}(\cos\theta)\,\mathrm{e}^{\mathrm{i}m\phi}. \quad (3)$$

We use the associated Legendre polynomials defined by the expression

$$P_\ell^m(x) \equiv \frac{(-1)^m}{2^\ell \ell!}\left(1-x^2\right)^{m/2}\frac{d^{\ell+m}}{dx^{\ell+m}}\left(x^2-1\right)^\ell, \quad (4)$$

where ℓ is the mode degree, and the azimuthal order m can have values from $-\ell$ to $+\ell$. A normalization constant in Eq. (1) is given by

$$N_\ell^m = (-1)^{\frac{m+|m|}{2}}\sqrt{\frac{2\ell+1}{4\pi}\frac{(\ell-|m|)!}{(\ell+|m|)!}}. \quad (5)$$

The pulsation velocity field in the stellar reference frame is found by differentiating the Lagrangian displacement vector

$$\boldsymbol{V} = \frac{\partial\boldsymbol{\xi}}{\partial t} = i\omega\boldsymbol{\xi}. \quad (6)$$

Substituting description (1) of the displacement vector into Eq. (6) we can express the three components of the velocity field vector $\boldsymbol{V} \equiv \left\{V_\mathrm{r}, V_\theta, V_\phi\right\}$ as

$$\left.\begin{aligned} V_\mathrm{r} &= v_\mathrm{p} R_{\ell m}(\cos\theta)\sin(m\phi+\omega t+\chi_0)\\ V_\theta &= v_\mathrm{p} M_{\ell m}(\cos\theta)\sin(m\phi+\omega t+\chi_0)\\ V_\phi &= v_\mathrm{p} L_{\ell m}(\cos\theta)\cos(m\phi+\omega t+\chi_0)\end{aligned}\right\}, \quad (7)$$

where $v_\mathrm{p} \equiv \sigma_r\omega$ and the auxiliary quantities $R_{\ell m}$, $M_{\ell m}$ and $L_{\ell m}$ contain only latitudinal dependence of the pulsation field and are specified by the associate Legendre polynomial $P_\ell^{|m|}(\cos\theta)$ and its θ derivative

$$\left.\begin{aligned} R_{\ell m}(\cos\theta) &= -N_\ell^m P_\ell^{|m|}(\cos\theta)\\ M_{\ell m}(\cos\theta) &= -KN_\ell^m\frac{\partial}{\partial\theta}P_\ell^{|m|}(\cos\theta)\\ L_{\ell m}(\cos\theta) &= -mKN_\ell^m\frac{P_\ell^{|m|}(\cos\theta)}{\sin\theta}\end{aligned}\right\}. \quad (8)$$

Using trivial trigonometric identities we separate the temporal and azimuthal dependency in Eq. (7) and represent a time-dependent pulsation velocity field as a superposition of the time-independent surface velocity maps, $\boldsymbol{V}^\mathrm{c} \equiv \left\{V_r^\mathrm{c}, V_\theta^\mathrm{c}, V_\phi^\mathrm{c}\right\}$ and $\boldsymbol{V}^\mathrm{s} \equiv \left\{V_r^\mathrm{s}, V_\theta^\mathrm{s}, V_\phi^\mathrm{s}\right\}$, multiplied by $\cos(\omega t+\chi_0)$ and $\sin(\omega t+\chi_0)$ respectively,

$$\boldsymbol{V} = \boldsymbol{V}^\mathrm{c}\cos(\omega t+\chi_0) + \boldsymbol{V}^\mathrm{s}\sin(\omega t+\chi_0). \quad (9)$$

Combining this formula with Eq. (7) we rewrite the total velocity field $\boldsymbol{V}$ as

$$\begin{aligned}\begin{pmatrix} V_\mathrm{r}\\ V_\theta\\ V_\phi\end{pmatrix} &= \begin{pmatrix} V_r^\mathrm{c}\\ V_\theta^\mathrm{c}\\ V_\phi^\mathrm{c}\end{pmatrix}\cos(\omega t+\chi_0) + \begin{pmatrix} V_r^\mathrm{s}\\ V_\theta^\mathrm{s}\\ V_\phi^\mathrm{s}\end{pmatrix}\sin(\omega t+\chi_0)\\ &= v_\mathrm{p}\begin{pmatrix} R_{\ell m}(\cos\theta)\sin(m\phi)\\ M_{\ell m}(\cos\theta)\sin(m\phi)\\ L_{\ell m}(\cos\theta)\cos(m\phi)\end{pmatrix}\cos(\omega t+\chi_0)\\ &\quad + v_\mathrm{p}\begin{pmatrix} R_{\ell m}(\cos\theta)\cos(m\phi)\\ M_{\ell m}(\cos\theta)\cos(m\phi)\\ -L_{\ell m}(\cos\theta)\sin(m\phi)\end{pmatrix}\sin(\omega t+\chi_0).\end{aligned} \quad (10)$$

Although Eq. (10) describes velocity field for a star pulsating in a single normal mode in the limit of no rotation, Eq. (9) is, in fact, more general and can be used for monoperiodic pulsations with considerably more complicated geometry. For instance, oblique non-radial modes of roAp stars can be described as a superposition of the spherical harmonic components aligned with the stellar axis of rotation (Bigot & Dziembowski 2002)

$$Y_\ell^m(\theta',\phi') = \sum_{k=-\ell}^{\ell} d_{m,k}^{(\ell)}(\delta) Y_\ell^k(\theta,\phi), \quad (11)$$

where the spherical harmonic transformation matrix $d_{m,k}^{(\ell)}(\delta)$ can be found in, e.g., Aerts et al. (1992). Thus, oblique non-radial pulsations are represented in the stellar reference frame as a sum of the harmonic components with different azimuthal numbers m. At the same time, magnetic perturbation of the non-radial modes in roAp stars (Shibahashi & Takata 1993; Saio & Gautschy 2004) and distortion of the pulsation geometry in normal rapidly rotating stars (Lee & Saio 1990) lead to the coupling of the spherical harmonics with different angular degree ℓ. All these effects can be accounted for by a straightforward generalization of Eqs. (1) and (9)

$$\overline{\boldsymbol{\xi}} = \mathrm{e}^{\mathrm{i}\omega t+\chi_0}\left\{1, K\frac{\partial}{\partial\theta}, K\frac{1}{\sin\theta}\frac{\partial}{\partial\phi}\right\}\sum_{\ell=1}^{N}\sum_{m=-\ell}^{\ell}\sigma_r^{\ell m} N_\ell^m Y_\ell^k(\theta,\phi) \quad (12)$$

and

$$\overline{\boldsymbol{V}} = \cos(\omega t+\chi_0)\sum_{\ell,m}\boldsymbol{V}_{\ell,m}^\mathrm{c} + \sin(\omega t+\chi_0)\sum_{\ell,m}\boldsymbol{V}_{\ell,m}^\mathrm{s}. \quad (13)$$

Additional horizontal motions due to the toroidal velocity components can also be included in Eq. (12) but are omitted here for the sake of brevity.

In the rest of the paper we use formula (9) acknowledging that, in general, velocity amplitudes $\boldsymbol{V}^{\rm c}$ and $\boldsymbol{V}^{\rm s}$ may contain contributions of the spherical harmonic components with various ℓ and m values. As a consequence, no simple relation can be established between the vector components of each of the velocity amplitude maps. Thus, in the most general case, all six scalar surface distributions forming the two vector fields $\boldsymbol{V}^{\rm c}$ and $\boldsymbol{V}^{\rm s}$ have to be treated as independent maps and reconstructed simultaneously in a self-consistent manner.

3. Line profile synthesis

The only observable characteristic of the pulsation velocity field is given by its projection onto the observer's line of sight,

$$\begin{aligned} V'_{\rm puls} \;=\; & -V_{\rm r}(\cos\theta\cos i + \sin\theta\cos(\phi+\varphi)\sin i) \\ & -V_\theta(\sin\theta\cos i - \cos\theta\cos(\phi+\varphi)\sin i) \\ & +V_\phi \sin i \sin(\phi+\varphi), \end{aligned} \tag{14}$$

where φ represents the stellar rotation phase and inclination i is the angle between the rotation axis and the line of sight. A velocity field describing the uniform rotation of a star,

$$V'_{\rm rot} = v_{\rm e}\sin i\sin\theta\sin(\phi+\varphi), \tag{15}$$

is added to $V'_{\rm puls}$ to form the total velocity component in the observer's reference frame.

The surface structure of pulsational fluctuations enters the line profile synthesis through the integration of local line profiles over the visible stellar hemisphere, which for a given rotation phase and wavelength λ can be written as

$$I^\star_{\rm calc}(\lambda,\varphi) = \frac{\int\int I_{\rm L}[M,\varepsilon,\lambda+\Delta\lambda_{\rm D}(M,\varphi)]\mu{\rm d}M}{\int\int I_{\rm C}(M)\mu{\rm d}M}. \tag{16}$$

Here $I_{\rm L}$ and $I_{\rm C}$ are the line and continuum intensities, M is the position on the stellar surface specified by latitude and longitude, μ is the cosine of the angle between the normal to the surface at M and the line of sight and $\Delta\lambda_{\rm D}(M,\varphi)$ is the total Doppler shift of the surface element M due to the stellar rotation and pulsation. We aim at describing line profile variability in stars with inhomogeneous abundance distribution, thus a surface chemical abundance map ε may enter in Eq. (16) as an additional independent surface parameter.

Local line profiles are computed numerically, using `ATLAS9` stellar model atmospheres (Kurucz 1993) and employing an accurate and fast scalar version of the quadratic DELO algorithm (Socas-Navarro et al. 2000) for the integration of the radiative transfer equation assuming LTE. Calculation of the line and continuous opacities is based on the routines implemented in the `SYNTH` code (Piskunov 1992). Our line profile synthesis neglects variation of the atmospheric structure over the stellar surface and during pulsation cycle. Pulsational distortion of the stellar surface geometry is also disregarded.

Modelling of modern high-resolution time-resolved observations of pulsating stars requires an analysis of up to a few thousand spectra simultaneously. Furthermore, computing local line profiles for, typically, several thousand surface zones at each pulsation phase is imperative for an accurate representation of the line profile variability of a rapidly rotating star and an adequate sampling of the surface pulsation velocity structures. Thus, the total of $\sim 10^6$ line profile evaluations are needed at each stage of the iterative fit of the theoretical spectra to observations of a single stellar spectral line. To make such problem tractable and to extend Doppler imaging analysis to modelling several lines simultaneously without compromising accuracy of the theoretical computations we have chosen to precompute a table of local line profiles for a set of μ values and a range of chemical abundances. Local line profiles required for numerical evaluation of Eq. (16) are determined by a linear interpolation within this table. For the calculations described in this paper we used a local profile table computed for 20 μ values spanning between 0.05 and 1.0. Each absorption profile is sampled with a step of 6×10^{-3} Å in wavelength. Mathematical properties of Eq. (16) allow us to interchange the order of disk-integration and convolution with an instrumental profile and to save computing time by carrying out the latter step already at the stage of local line profile tabulation.

4. Imaging of the pulsation velocity field

The surface pulsational fluctuations lead to characteristic distortions in the profiles of Doppler-broadened stellar spectral lines. During oscillation cycle and in the course of stellar rotation these distortions will move across line profiles due to changes of the visibility and projected Doppler shifts of individual zones at the stellar surface. In the pulsation Doppler imaging technique we utilize the information contained in both the pulsational variability of stellar line profiles and in the rotational modulation of this variability pattern. Our DI code reconstructs pulsation features at the surfaces of stars by inverting a time series of high-resolution spectra into a time-dependent velocity map of the stellar surface. Mathematically the inverse problem of pulsation Doppler imaging is solved by minimizing the error function:

$$\begin{aligned} E \;=\; & \sum_t\sum_\lambda \left[I^\star_{\rm calc}(\lambda,t,\boldsymbol{V}^{\rm c},\boldsymbol{V}^{\rm s}) - I^\star_{\rm obs}(\lambda,t)\right]^2/\sigma^2_{\rm obs}(\lambda,t) \\ & +R(\boldsymbol{V}^{\rm c},\boldsymbol{V}^{\rm s}) \end{aligned} \tag{17}$$

which characterizes the discrepancy between computed profiles $I^\star_{\rm calc}(\lambda,t,\boldsymbol{V}^{\rm c},\boldsymbol{V}^{\rm s})$ and the observed stellar spectra $I^\star_{\rm obs}(\lambda,t)$. The summation in Eq. (17) is weighted by the error bars $\sigma_{\rm obs}(\lambda,t)$ of the observed profiles and is carried out over all wavelengths λ and moments of observation t.

Similar to other applications of the Doppler mapping technique, an inversion of the pulsation velocity field is a fundamentally ill-posed problem. Due to inevitable imperfections of real observational data, such as random noise, gaps in phase coverage, and intrinsic limitations of the DI inversion procedure, an infinite number of solutions will be able to fit observations within the error limits. However, the majority of these solution are deemed unrealistic because they exhibit large fluctuations over small distances and will be unstable with respect to the initial guess of a surface map. To find a unique solution and ensure a consistency between the number of free parameters and information contained in observational data the inverse problem must be *regularized*, meaning that a solution will be sought only within a restricted set of the surface distributions

selected following some additional criteria. Mathematically a uniqueness and stability of the solution can only be achieved by including the regularization function $R(\boldsymbol{V}^{\rm c}, \boldsymbol{V}^{\rm s})$ in the total error function defined by Eq. (17). The regularization procedure ensures that the pulsation amplitude maps $\boldsymbol{V}^{\rm c}$ and $\boldsymbol{V}^{\rm s}$ derived by the DI code are the simplest or smoothest distributions among infinite number of solutions providing an adequate fit to available observational data.

Two different types of regularization functions are commonly employed in the surface mapping. One, the so-called Maximum Entropy Method (MEM), maximizes configurational entropy of a surface image and is widely used to recover complex temperature (Vogt et al. 1987) and magnetic (Brown et al. 1991) inhomogeneities at the surfaces of late-type active stars. An alternative Tikhonov regularization technique (Tikhonov 1963) provides a measure of a smoothness of the surface distribution and acts locally by imposing a correlation between neighbouring pixels of a surface image. This regularization method is often applied in investigations of the geometries of abundance spots in chemically peculiar magnetic stars (e.g. Lüftinger et al. 2003). The studies by Piskunov (1990) and Strassmeier et al. (1991) indicated that the specific form of regularization function becomes irrelevant in mapping spots of temperature or chemical composition when rotational modulation of stellar line profiles is large compared to the noise in observed spectra. However, Piskunov & Kochukhov (2002) have demonstrated that performance of the two regularization strategies is fundamentally different in mapping the global well-ordered surface structures, for instance dipolar-like magnetic fields in chemically peculiar stars or, in the context of the present paper, surface pulsational distortions in oscillating stars. Both types of surface structures are characterized by large-scale deviations from the average value of a parameter of interest and, compared to other solutions permitted by the observational data, do not have minimal information content sought by the Maximum Entropy. Consequently, global magnetic field geometries and stellar pulsation maps cannot be recovered by a MEM-based inversion code. Taking this into account, for the present Doppler imaging investigation of stellar pulsations we use the Tikhonov regularization functional defined with the expression

$$R(\boldsymbol{V}^{\rm c}, \boldsymbol{V}^{\rm s}) = \Lambda_{\rm c} \int\int \sum_{k=1}^{3} \left\| \nabla V_k^{\rm c}(M) \right\|^2 {\rm d}M + \Lambda_{\rm s} \int\int \sum_{k=1}^{3} \left\| \nabla V_k^{\rm s}(M) \right\|^2 {\rm d}M, \quad (18)$$

where $\Lambda_{\rm c,s}$ are the regularization parameters and index k runs over all vector components of the pulsation maps $\boldsymbol{V}^{\rm c}$ and $\boldsymbol{V}^{\rm s}$.

For the general problem of recovering the vector distributions of pulsation velocity amplitudes our Doppler imaging code reconstructs the 6 independent surface maps using a conjugate gradient minimization algorithm. The value of a pulsation amplitude in each surface zone is treated as an independent quantity and is related to pulsation parameters in the nearby surface elements only through the regularization procedure. Thus, our pulsation Doppler mapping technique is truly free from any a priori assumptions about geometry of the surface pulsational fluctuations. The method is applicable to all types of stellar pulsations provided that the corresponding line profile variability is dominated by the velocity field rather than pulsational changes of the atmospheric structure.

5. Numerical tests of the inversion code

Numerical experiments provide the most straightforward and reliable way to test performance of a Doppler imaging code under realistic conditions. In the numerical tests described in this section we use the new DI code in the forward mode to calculate line profile variability for a given pulsation amplitude map. These synthetic spectra are convolved with the instrumental profile and a random noise component is added to simulate imperfections of real observational data. The code then uses simulated observations to recover velocity maps and resulting surface images are analysed to assess the range of stellar and pulsation parameters where robust recovery of the pulsation geometry can be expected.

In simulations presented in this paper we limit pulsational mapping to the reconstruction of the vertical components, $V_r^{\rm c}$ and $V_r^{\rm s}$, of the pulsation amplitude vectors. The assumption of the dominance of the vertical pulsational fluctuations is justified for many types of oscillating stars. In particular, it is well-suited for the high-overtone p-mode pulsations in roAp stars, which will comprise the first targets for application of our code. At the same time, we also plan to assess possibility to recover the structure of horizontal pulsation disturbances in a separate future investigation.

Tests of the pulsation velocity inversions are based on modelling variations of the Nd III 6145.07 Å line. This feature is one of the most useful spectroscopic diagnostics of the roAp pulsations (e.g. Kochukhov & Ryabchikova 2001). Synthetic spectra were computed using the ATLAS9 model atmosphere with $T_{\rm eff} = 8000$ K and $\log g = 4.0$ and a homogeneous Nd abundance of $\log(N_{\rm Nd}/N_{\rm tot}) = -6.5$. The projected stellar rotational velocity $v_{\rm e} \sin i = 40$ km s^{-1} and the pulsation parameter[1] $v_{\rm p} = 10$ km s^{-1} were adopted in all simulations. The disk-integrated stellar line profiles are evaluated using a 1800-element grid formed by rectangular surface zones $6^\circ \times 6^\circ$ each. Spectra are convolved with a Gaussian instrumental profile corresponding to the resolution of $\lambda/\Delta\lambda = 123\,000$ and a $S/N = 300$ noise component is added. Each type of the pulsation geometry considered here was recovered using 500 spectra sampling a single stellar rotation cycle and approximately 64 pulsation cycles (i.e., we use the pulsation to rotation frequency ratio of $\omega/\Omega \approx 64$). Inversions were carried out for three values of the stellar inclination angle, $i = 35^\circ$, 60° and 85°.

In the following we discuss some of the reconstruction results in more detail. Pulsation maps recovered with the new DI technique are presented in Figs. 3–9 and 11, 12, while Figs. 2 and 10 illustrate the respective pulsational line profile

[1] Note that the actual physical pulsation velocities at the stellar surface are always smaller than the $v_{\rm p}$ adopted here and do not exceed 5 km s^{-1} for most of the studied pulsation modes.

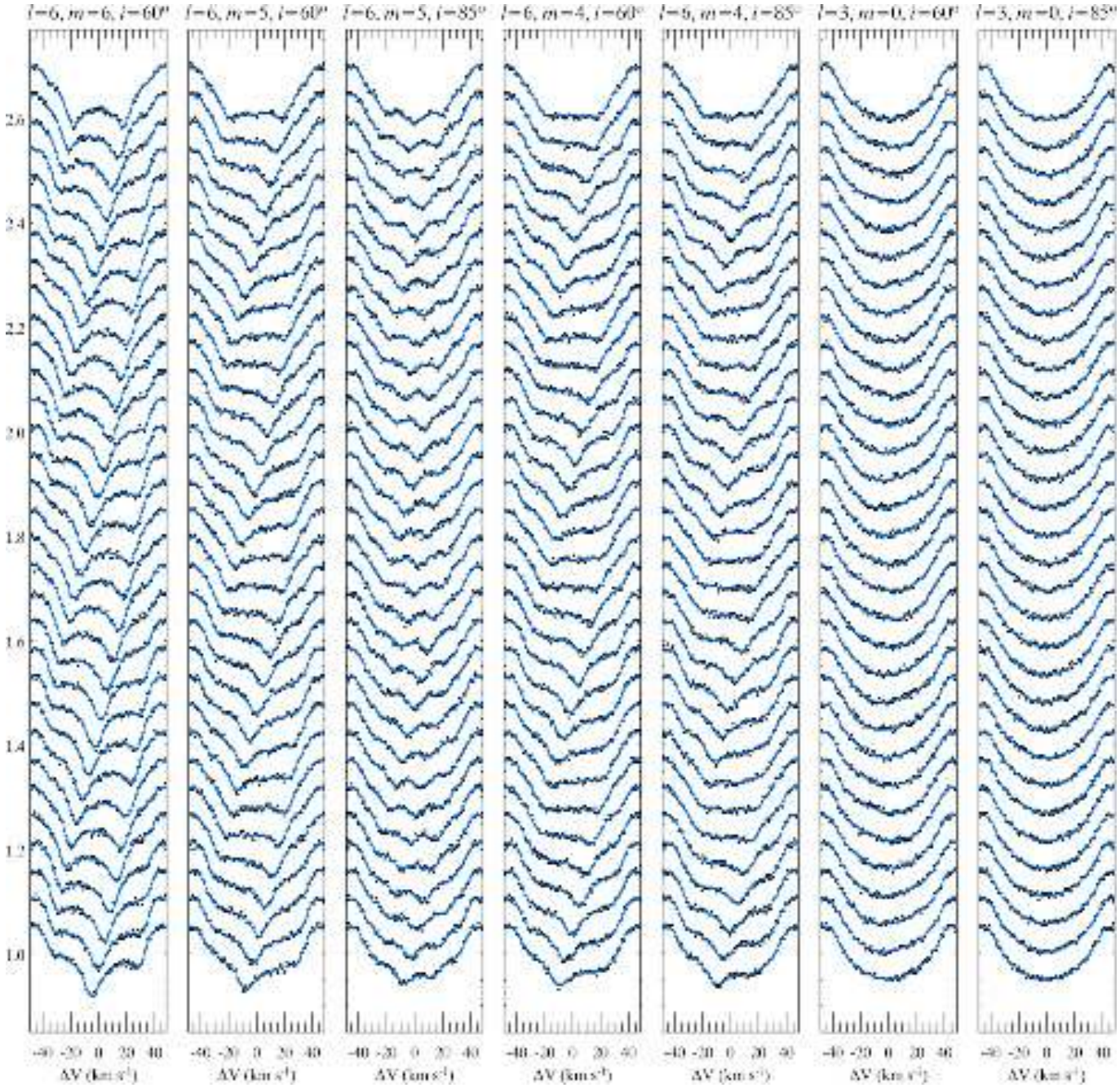

Fig. 2. Line profile variability due to different combinations of the stellar inclination and pulsation modes. Symbols show simulated observational data and solid lines illustrate the fit by the pulsation Doppler imaging code. Each column shows the first 32 profiles (out of 500 spectra used in numerical tests) covering about 3 oscillation cycles with a step of ≈13% of the pulsation period. Spectra for consecutive pulsation phases are shifted in the vertical direction.

variability and give an impression of the quality of the fit to simulated observations achieved by the DI code.

5.1. Sectoral mode

In the first test with the pulsation DI code we reconstructed a sectoral pulsation structure corresponding to the $\ell = 6$, $m = 6$ oscillation mode. This pulsation geometry is arguably the easiest surface pattern to image since it involves only one row of periodic surface fluctuations and is characterized by a high-amplitude line profile variability (Fig. 2) for large and intermediate inclination angles. Figure 3 presents velocity maps recovered from the spectra simulated for $i = 60°$. The quality of reconstruction is good over most of the visible stellar surface. The sectoral $\ell = m = 6$ structure is easily recognizable in both the V_r^c and V_r^s maps and finds a satisfactory agreement with the input velocity distribution.

For the inclination angle $i = 60°$ and lower values the surface pulsation structure appears to be shifted to higher stellar latitudes. This reflects the fact that DI technique is primarily

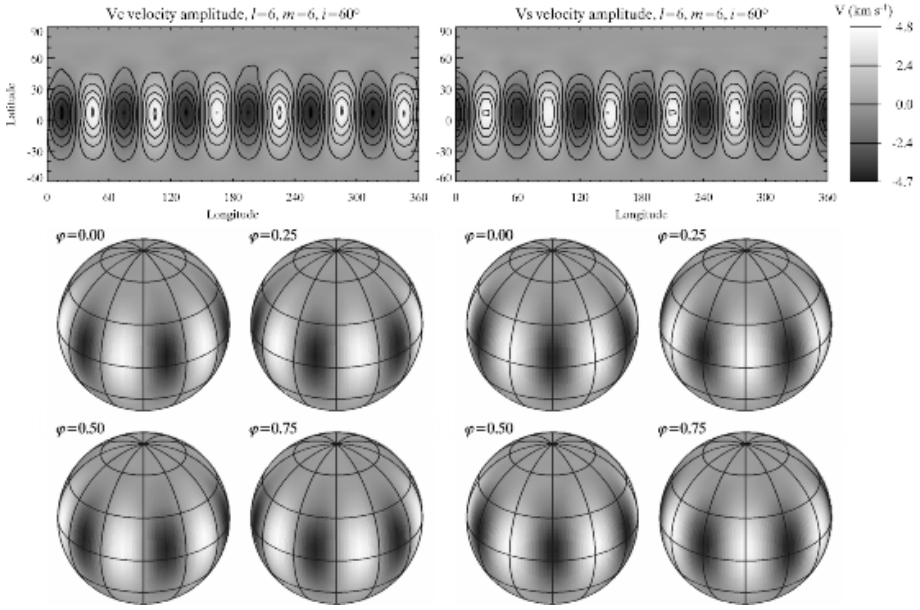

Fig. 3. Doppler imaging reconstruction of the pulsation velocity field for the sectoral $\ell = m = 6$ mode and inclination angle $i = 60°$. Rectangular projections of the vertical pulsation velocity amplitudes, $V_r^{\rm c}$ and $V_r^{\rm s}$, are shown as greyscale images in the upper panels. The contours of equal velocity amplitude are plotted over the rectangular greyscale images with a step of 1.0 km s^{-1}. The spherical projections of the respective pulsational amplitude maps are plotted below. In the spherical plots the star is shown at four different aspect angles, corresponding to the rotation phases $\varphi = 0.00$, 0.25, 0.50 and 0.75, and $i = 60°$. The grid at the stellar surface is plotted with a 30° step in longitude and latitude.

sensitive to the surface patterns located not far from the sub-observer latitude, but have difficulties recovering subequatorial structures. We stress that this problem is not due to a bias introduced by a regularization procedure but stems from a fundamental intrinsic limitation of the surface mapping method.

5.2. Antisymmetric tesseral mode

The $\ell = 6$, $m = 5$ pulsation mode was investigated as an example of the antisymmetric tesseral pulsations. The surface velocity fluctuations for this mode are limited to latitudes below 60° and are antisymmetric with respect to the rotational equator. The line profile variations for the inclination angles $i = 60°$ and 85° are shown in Fig. 2, while Figs. 4 and 5 present the surface velocity images recovered by the DI code. These maps testify that velocity inversion was successful despite challenging properties of the input surface pattern. The reconstruction results for $i = 60°$ demonstrate poorer recovery of the subequatorial structures. Nevertheless, this does not hamper the mode identification and, furthermore, this bias disappears for $i = 85°$ when both stellar hemispheres have comparable contribution to the disk-integrated line profiles.

Remarkable success of the pulsation velocity mapping of the antisymmetric tesseral pattern provides a convincing illustration of the advantages of our DI method compared to the temperature imaging of pulsations proposed by BTK. The latter authors were unable to recover an antisymmetric tesseral mode and argued that this failure is due to a mutual cancellation of the profile distortions corresponding to structures on different sides of the equator. However, such cancellation occurs only for temperature (or abundance) surface inhomogeneities but not for antisymmetric velocity structures. Even if i is close to 90° the wavelength contributions of such velocity structures are shifted in the opposite directions and, hence, do not coadd destructively. Consequently, our program does not encounter significant difficulties in deducing the true antisymmetric pulsation geometry.

Reconstructed images in Fig. 5 also reveal that, even for large stellar inclinations, the pulsation velocity mapping is not affected by the well-known effect of reflection of surface structures with respect to the rotational equator. This once again provides a clear example of substantial differences between mapping of a surface parameter (temperature or chemical abundance) which changes only the local line strength and a surface quantity responsible for velocity shifts of the local line profiles.

5.3. Symmetric tesseral mode

Symmetric tesseral pulsations represented by the $\ell = 6$, $m = 4$ mode is the most complex pulsation map considered in this paper. The respective surface structure consists of the three bands of periodic fluctuations, encircling the star at latitudes ±40° and 0° and symmetric relative to the equator.

The line profile variations for $i = 60°$ and 85° are illustrated in Fig. 2. Reconstruction results for these two stellar inclinations are shown in Figs. 6 and 7 respectively. As one can expect, the structures below the rotational equator are not properly recovered for low and intermediate inclination angles. This does not affect the mode identification since the pulsation structure in the northern hemisphere is restored nicely and can be unambiguously associated with the $\ell = 6$, $m = 4$ mode.

Pulsational mapping for the large inclination angle (Fig. 7) is able to recover the full symmetric tesseral pattern. However, a significant asymmetry in deduced velocity amplitudes is visible even for inclinations close to 90°. This has no bearing on assigning the correct ℓ and m numbers to the recovered pulsation pattern, but may create certain problems for accurate characterization of the harmonic constituents of the pulsation modes distorted by the stellar rotation or magnetic field.

5.4. Zonal mode

In addition to the reconstruction of complex non-axisymmetric tesseral and sectoral pulsation modes we investigated

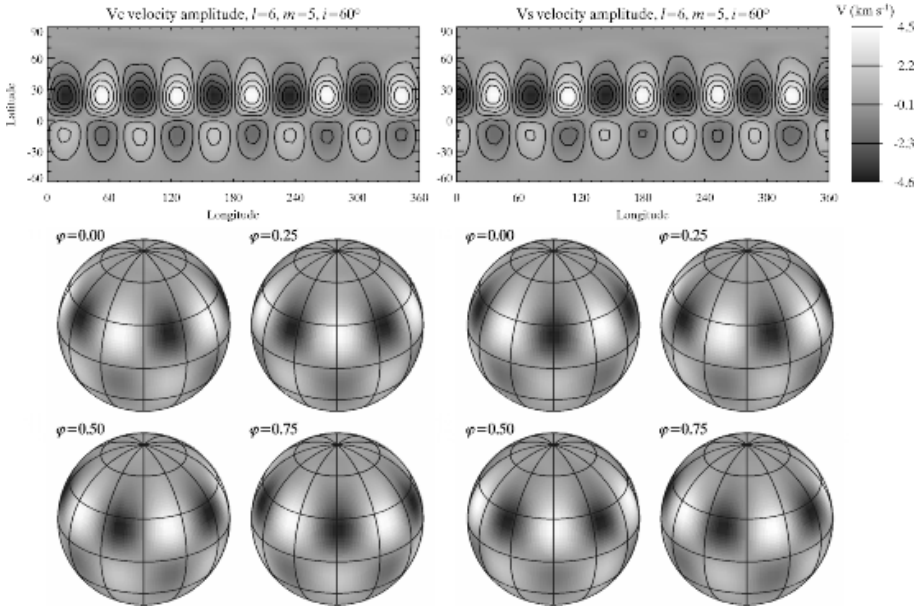

Fig. 4. Doppler imaging reconstruction of the pulsation velocity field for the antisymmetric tesseral $\ell = 6$, $m = 5$ mode and $i = 60°$.

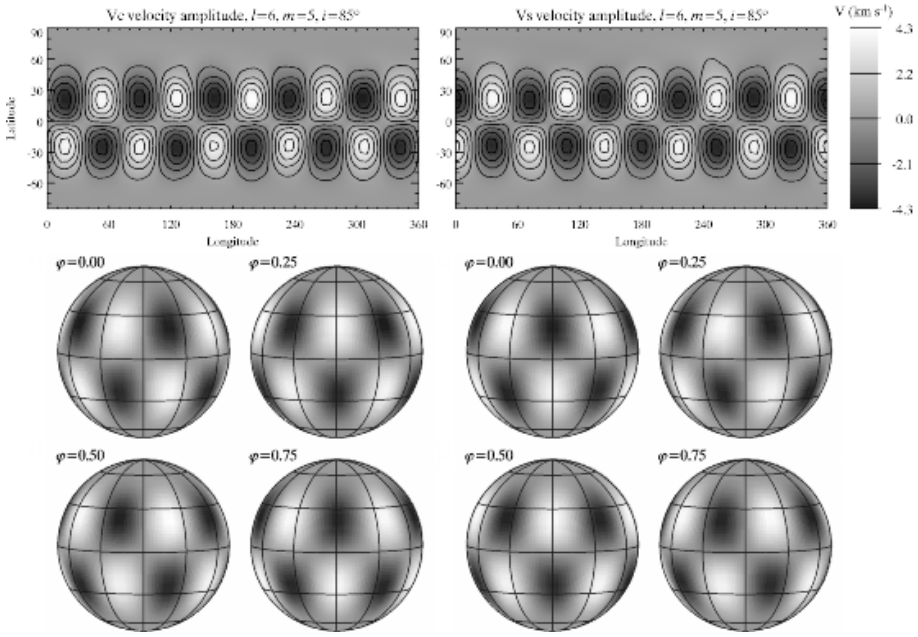

Fig. 5. Same as Fig. 4 for $i = 85°$.

capability of our technique to recover geometry of a zonal pulsation mode aligned with the stellar axis of rotation.

The $\ell = 3$, $m = 0$ pulsations result in marginal profile variability when the star is observed close to the equator (Fig. 2). However, the quality of the velocity field reconstruction is acceptable for low and intermediate inclinations. Axisymmetric pulsation structure is clearly revealed in the Doppler images presented in Fig. 8. As it follows from the description of the velocity field for axisymmetric non-radial pulsations given by Eq. (10), only one pulsation map ($\boldsymbol{V}^{\rm s}$) is needed for modelling pulsation variability, whereas the other map is null over the whole stellar surface (given that the phase constant χ_0 was chosen appropriately). In other words, axisymmetric velocity distributions do not exhibit surface variation of the pulsation phase except for the π radian phase jumps at the zonal node lines. Despite this simplified property of axisymmetric pulsations, we recovered both pulsation maps simultaneously using the same procedure as before. No spurious structures appear in the $V_r^{\rm c}$ map in Fig. 8 enabling us to conclude that the two pulsation amplitude maps are truly independent surface quantities and cannot be confused by the DI code.

Reconstruction of an equator-on axisymmetric pulsation geometry (Fig. 9) represents the most difficult case because contributions of pulsation disturbances above and below the rotational equator are antisymmetric for the $\ell = 3$ mode and are cancelled in the disk-integrated line profiles. As a result, very weak line profile variability is observed and the DI code significantly underestimates pulsation amplitudes at the poles and suffers from the problem of reflection of surface structures relative to the equator.

Spectroscopic variability due to axisymmetric pulsation modes or due to complex modes containing non-negligible

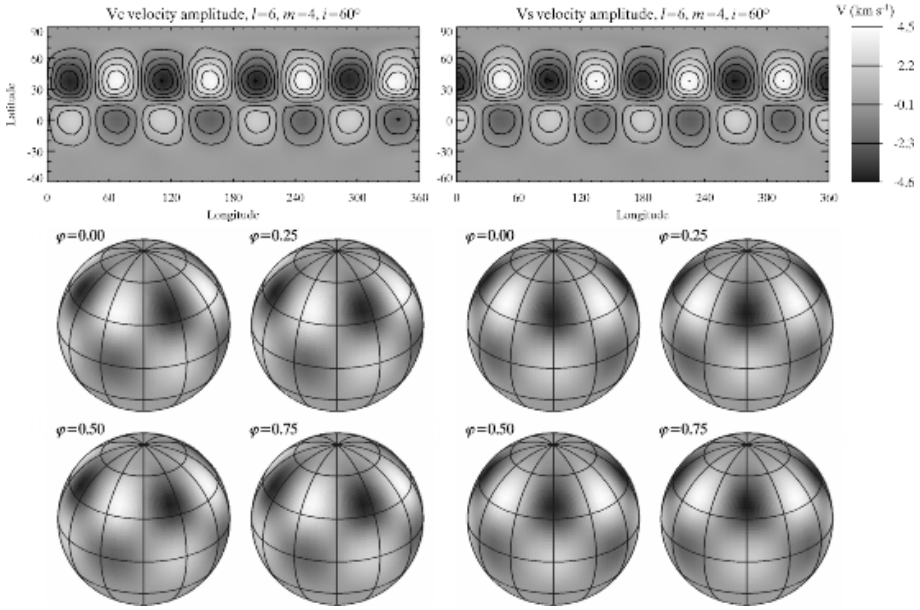

Fig. 6. Doppler imaging reconstruction of the pulsation velocity field for the symmetric tesseral $\ell = 6$, $m = 4$ mode and $i = 60°$.

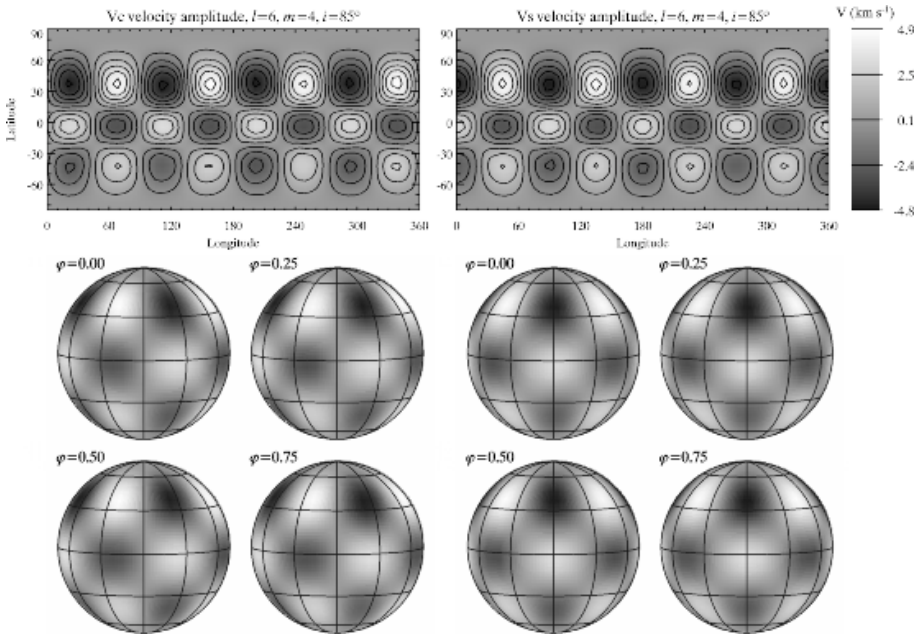

Fig. 7. Same as Fig. 6 for $i = 85°$.

axisymmetric components cannot be represented by the rotation of a surface pattern, which invalidates the method of the temperature stellar pulsational mapping proposed by BTK.

5.5. Oblique dipolar modes

The photometric pulsation variability due to the high-overtone p-modes in roAp stars is best described by the oblique pulsator model suggested by Kurtz (1982). Within the framework of this purely empirical hypothesis pulsations in roAp stars are attributed to axisymmetric $\ell = 1$ modes with their axis inclined with respect to the stellar axis of rotation and, possibly, aligned with the symmetry axis of a global magnetic field typical of roAp stars. Despite a certain success in interpreting photometric time series data the oblique pulsator model still lacks a satisfactory theoretical foundation and was never verified with spectroscopic observations. In fact, one of the most recent time-resolved high-dispersion observations of the best-studied roAp pulsator HR 3831 (Balona 2002) suggested that spectroscopic variability of this star is explained by a superposition of the several $\ell = 2$ harmonic components aligned with the rotation axis rather than produced by an oblique axisymmetric $\ell = 1$ mode. It is the primary aim of the present series of papers to develop a technique that can be used to reveal the true pulsation geometry of roAp stars and eventually to confirm or disprove the oblique pulsator model.

In addition to resolving the puzzle of roAp stars, spectroscopic modelling of oblique pulsations is also of great interest in a general context of research on non-radially oscillating stars due to the possibility to observe the same stellar oscillation mode at different aspect angles, which is very likely to provide much more stringent constraints for stellar

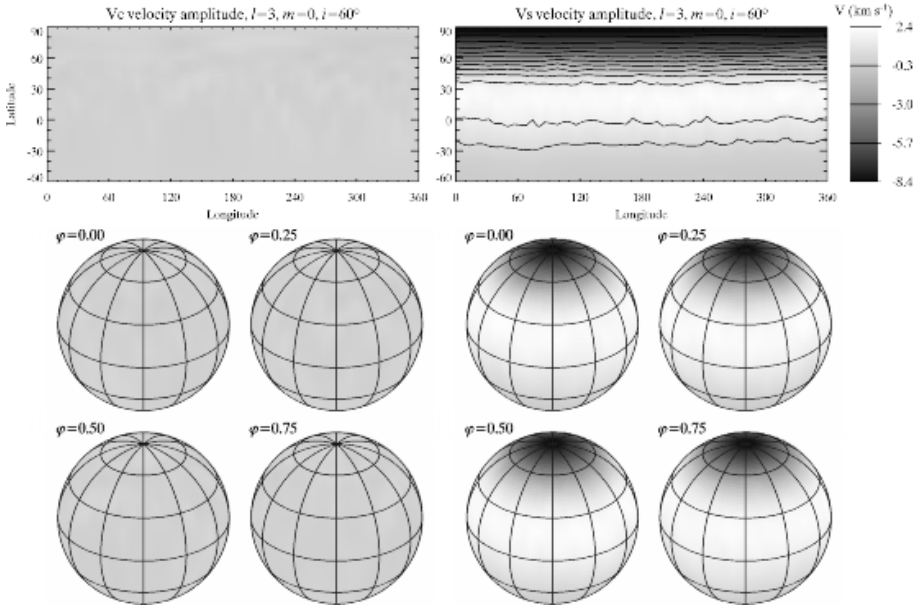

Fig. 8. Doppler imaging reconstruction of the pulsation velocity field for the zonal $\ell = 3$, $m = 0$ mode and $i = 60°$.

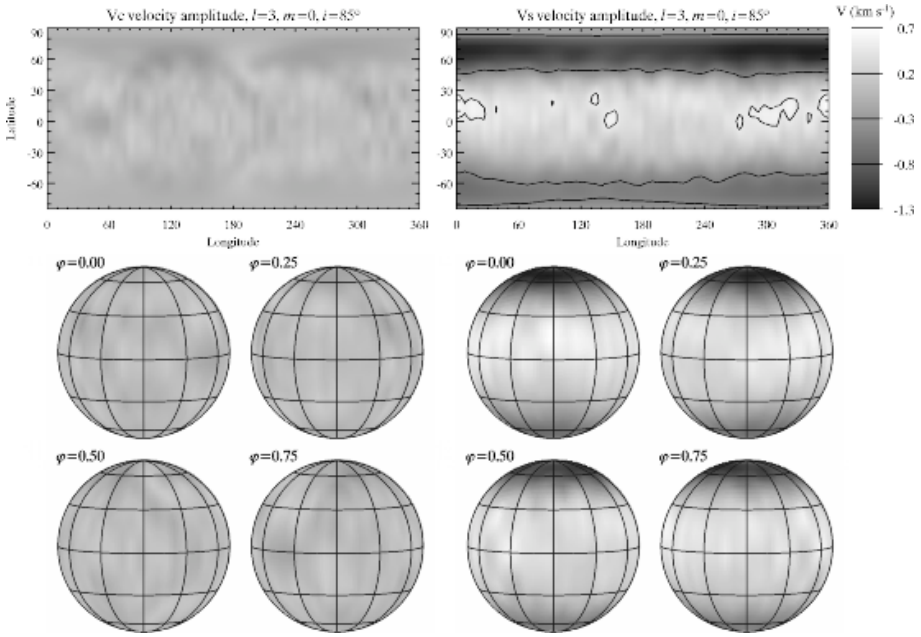

Fig. 9. Same as Fig. 8 for $i = 85°$.

pulsation geometry. It should be stressed that some characteristics of the profile variability in very slowly rotating roAp stars can be studied with the methods developed for normal pulsators (Kochukhov & Ryabchikova 2001). However, in a more general case when rotational Doppler shifts become comparable or larger than those produced by the pulsation disturbances, the properties of the total velocity field and the respective line profile variability are expected to be quite different compared to any single pulsation mode aligned with the rotation axis. Thus, it is important to study the effects due to oblique pulsation modes using a dedicated physical model and numerical methods specially designed for that purpose.

The first numerical simulations of the line profile changes due to oblique stellar non-radial pulsations were carried out by Baade & Weiss (1987) and Pesnell (1990). However, these early calculations were performed long before the pulsational line profile variability of roAp stars was actually discovered and characterized in detail (Kochukhov & Ryabchikova 2001). A coarse line formation model (neither of the two studies was based on local line profiles computed with a realistic stellar model atmosphere) or unrealistically large adopted pulsation amplitudes suggest that the results of Baade & Weiss (1987) and Pesnell (1990) have a limited relevance for interpreting modern time-resolved spectroscopic observations of roAp stars.

Here we present the first realistic calculations of the line profile variability for a roAp pulsator. We assume that pulsations are given by the $\ell = 1$, $m = 0$ mode inclined by the angle $\delta = 90°$ with respect to the rotation axis. The adopted pulsation parameter $v_\mathrm{p} = 10$ km s^{-1} results in maximum radial velocity semi-amplitude of $\approx$2 km s^{-1} which is comparable to the radial velocity variability observed in the roAp star

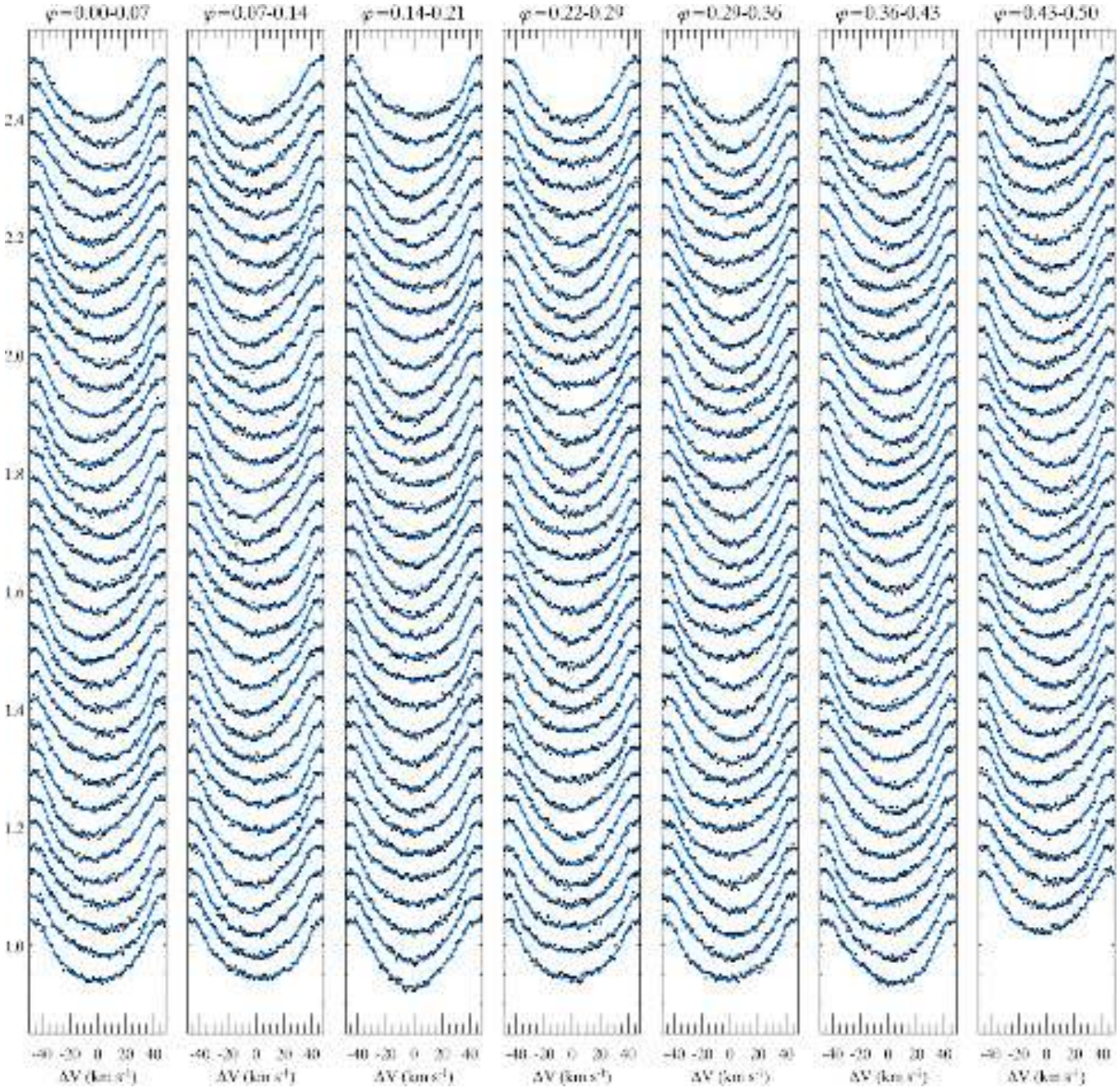

Fig. 10. Line profile variability due to the oblique $\ell = 1$, $m = 0$, $\delta = 90°$ pulsation mode for the star observed at the inclination angle $i = 60°$. Symbols show simulated observational data and solid lines illustrate the fit by the pulsation Doppler imaging code. 250 profiles presented in this figure cover half of the rotation cycle of the star (rotation phases $\varphi = 0.0$–0.5) and 32 oscillation cycles. Spectra for consecutive pulsation phases are shifted in the vertical direction. Note remarkably different character of the line profile variability at phases $\varphi = 0.0$ (or 0.5) and 0.25.

HR 3831 by Balona (2002). The pulsational profile variability of the Nd III 6145.07 Å line is presented in Fig. 10. This figure illustrates a remarkable rotational modulation of the line profile variation pattern, as expected for an oblique pulsator. For instance, at the rotation phases $\varphi \approx 0.0$ and 0.5, when the pulsation axis is nearly aligned with the line of sight, periodic changes of both the line centroid and the line width are evident. On the other hand, at $\varphi \approx 0.25$ the radial velocity variability is negligible and profile changes are mostly due to variation of the line width with pulsation cycle.

The DI code successfully recovers the oblique dipolar pulsation mode. The V_r^s pulsation map shows a clear dipolar pattern (see Fig. 11) and no spurious pulsation velocity structures appear in the V_r^c map. Figure 12 illustrates an attempt to restore the surface pulsation velocity field for the dipolar mode with the same characteristics as above, but inclined by the angle $\delta = 40°$ relative to the rotation axis. The overall quality of reconstruction is satisfactory: the program correctly identifies the location of the pulsation pole in the northern stellar hemisphere and deduces realistic pulsation amplitudes for all

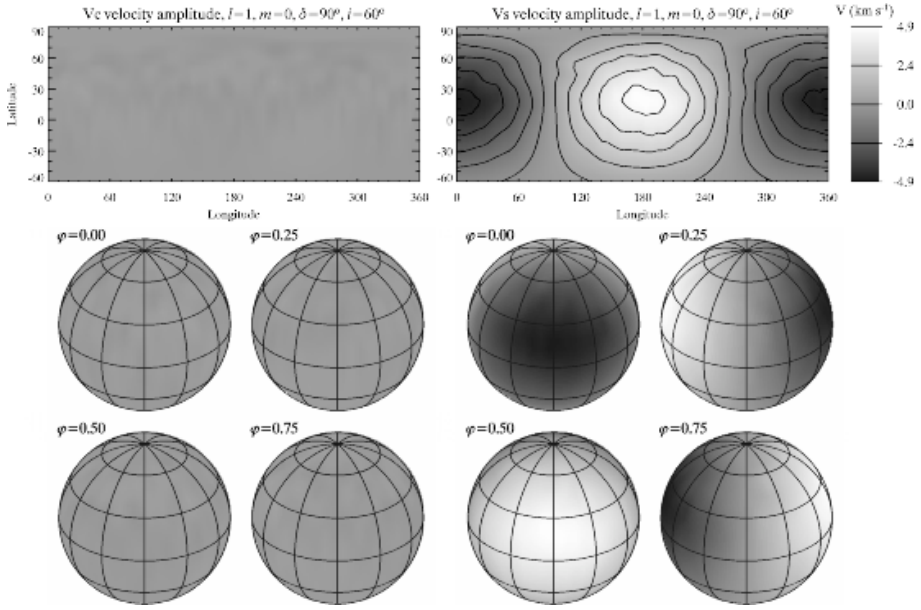

Fig. 11. Doppler imaging reconstruction of the pulsation velocity field for the oblique axisymmetric dipole mode ($\ell = 1$, $m = 0$, obliquity angle $\delta = 90°$) and $i = 60°$.

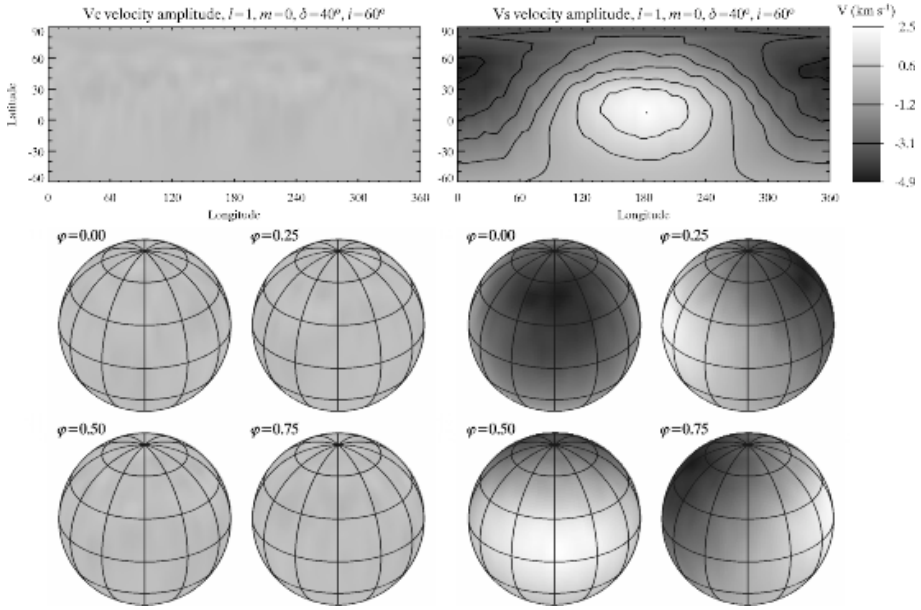

Fig. 12. Same as Fig. 11 for $\delta = 40°$.

but subequatorial stellar latitudes. This test enables us to conclude that the pulsational mapping technique can be used to obtain reliable velocity maps for pulsators with any obliquity value.

Finally, we note that an oblique axisymmetric $\ell = 1$ pulsation is equivalent to a superposition of the $\ell = 1, m = -1, 0, +1$ spherical harmonic components in the stellar reference frame. Since no single unique m value can be attributed to such a pulsation geometry, the pattern-rotation description suggested by BTK is not a viable alternative for investigation of oblique stellar pulsations.

6. Sensitivity to parameter errors

The fundamental stellar parameters as well as the quantities determining the stellar viewing geometry are required as an input for Doppler mapping of the pulsation velocity field, but are rarely known with high precision. In this section we investigate to what extent inevitable errors in the input parameters can degrade the recovered surface images and render the mapping results unreliable.

We note that the stellar atmospheric parameters, such as $T_{\rm eff}$, log g, micro- and macroturbulent broadening, mainly affect the strength and shape of the local line profiles. Moderate errors in these parameters lead to a poorer fit to the observed spectra but are unlikely to distort the surface pattern geometry, at least for those rapidly rotating stars where the Doppler broadening dominates and the local line profile shape becomes unimportant. Similarly, degradation of the quality of the input spectra in the form of a reduced *S/N* and resolving power, as well as unrecognized blending of the spectral features selected for the pulsational diagnosis, will result in predictable gradual loss of resolution and detail in the surface maps. On the other hand, another, geometrical, group of the input parameters, the

inclination angle i and the projected rotational velocity $v_e \sin i$, are critical for all types of the stellar surface imaging since these quantities define the mapping relation between the surface location of inhomogeneities and the wavelength position of the respective distortions in the Doppler-broadened spectral line profiles. An impact of the deviations of the geometrical parameters from their optimal values is non-trivial in any Doppler imaging application and has to be investigated here anew given the existence of significant differences in the properties of the velocity and temperature (or chemical abundance) surface mapping.

In this section we assess sensitivity of the velocity mapping procedure to errors in $v_e \sin i$ and i. Test inversions with incorrectly assumed input parameters are carried out for the sectoral $\ell = 6$, $m = 6$ and the symmetric tesseral $\ell = 6$, $m = 4$ pulsation modes. The respective simulated observations are computed with $v_e \sin i = 40$ km s^{-1} and $i = 60°$. Reconstructions of these velocity distributions using correct parameters were presented in Figs. 3, 6 and were discussed in Sects. 5.1 and 5.3.

6.1. Projected rotational velocity

Sensitivity to errors in the rotational velocity was studied by adopting $v_e \sin i = 38$ and 42 km s^{-1} in reconstruction of the chosen pulsation modes. Results of these inversions are illustrated in Fig. 13. The structure of the sectoral pulsation velocity pattern is noticeably distorted by a 5% underestimate of $v_e \sin i$. The velocity fluctuations for the sectoral $\ell = 6$ mode are already located in the areas of maximal rotational Doppler shift and, if $v_e \sin i$ is underestimated, the DI code is forced to compress the pulsation pattern in latitude and increase the respective local velocity amplitude. The three other tests presented in Fig. 13 are characterized by a moderate distortion of the pulsation geometry. We find that, where possible, the DI code attempts to compensate an error in $v_e \sin i$ by changing the latitudinal position of pulsational fluctuations. In this way errors in the projected rotational velocity result in shifting of the most important pulsation structures into (for an underestimated $v_e \sin i$) or out of (for too large a $v_e \sin i$) the surface zones with large rotational Doppler shift. This behaviour of the pulsational Doppler mapping procedure is quite different from the bias introduced by a wrong $v_e \sin i$ value into the scalar temperature or chemical abundance maps reconstructed with regular DI codes. There underestimating of the projected rotational velocity leads to appearance of a low-latitude band of high temperature or elemental abundance, while overestimating results in an opposite effect. No such spurious rotationally symmetric structures can appear in pulsation velocity images because the very formulation of the velocity mapping problem excludes possibility of introducing a stationary velocity component during the iterative fit. Consequently, latitude shifts of pulsation pattern and some changes of the local values of oscillation amplitude remain the only effects induced by $v_e \sin i$ errors.

We stress that even by introducing spurious distortions in the pulsation maps the DI code is unable to obtain a good fit to the input spectra: all maps shown in Fig. 13 give about 60% larger average deviation compared to the respective reconstructions using the correct $v_e \sin i$ parameter. This suggests that the rotational velocity can be deduced to within a few % of the true value by optimizing the fit to the observed spectra.

6.2. Stellar inclination

Reconstructions of the pulsation velocity patterns for incorrect inclination angle are presented in Fig. 14. In these tests we adopted $i = 40°$ and 80°, which deviates by $\mp 20°$ from the inclination angle used to generate the input spectra. It is clear than even such large uncertainty in the inclination angle does not significantly distort the recovered pulsation geometry or latitudinal positions of the surface structures. Thus, identification of the normal modes is insensitive to large errors in the stellar inclination. The quality of the fit to observations is unaffected as well.

At the same time, we find some influence on the physical information extracted by our code, namely the local pulsation amplitudes. In particular, the DI code tends to derive larger pulsation amplitude for the structures corresponding to the sectoral pattern if i is underestimated and lower amplitude for too large an inclination angle. This bias is easy to explain: for underestimated (overestimated) i the visibility of the equatorial pattern of the sectoral $\ell = 6$ pulsation is decreased (increased), hence the code compensates an incorrect inclination angle by, respectively, increasing (decreasing) the absolute value of the local pulsation amplitude. The trend is reversed for the symmetric tesseral $\ell = 6$, $m = 4$ mode since the respective velocity pattern with main contribution to the disk-integrated line profiles is located at intermediate latitudes.

7. Conclusions

We presented a novel variety of the Doppler imaging technique that can be used to obtain an in-depth information about the surface geometry of the stellar pulsational fluctuations. The line profile variability of non-radial stellar pulsators is modelled in terms of an inhomogeneous and time-dependent surface distribution of the pulsation velocity field. In reconstructing a two-dimensional image of the stellar oscillation pattern we do not impose any a priori restrictions on the shape of the pulsation geometry, in particular we avoid explicit or implicit parameterization of pulsations with the spherical harmonic functions. This unique feature of our approach makes possible, for the first time, an objective study of different types of stellar non-radial pulsations with complex surface distribution of pulsational disturbances, for example oblique and magnetically distorted non-radial pulsations in roAp stars and non-radial modes in normal stars perturbed by the rapid stellar rotation.

It is demonstrated that the previously suggested method of temperature mapping of stellar non-radial pulsations (Berdyugina et al. 2003) implicitly assumes a restricted spherical harmonic pulsation geometry and fails to address the problem of modelling the pulsational line profile variation dominated by the velocity fluctuations.

Performance and limitations of the new Doppler mapping technique are investigated with numerical tests. Reconstruction

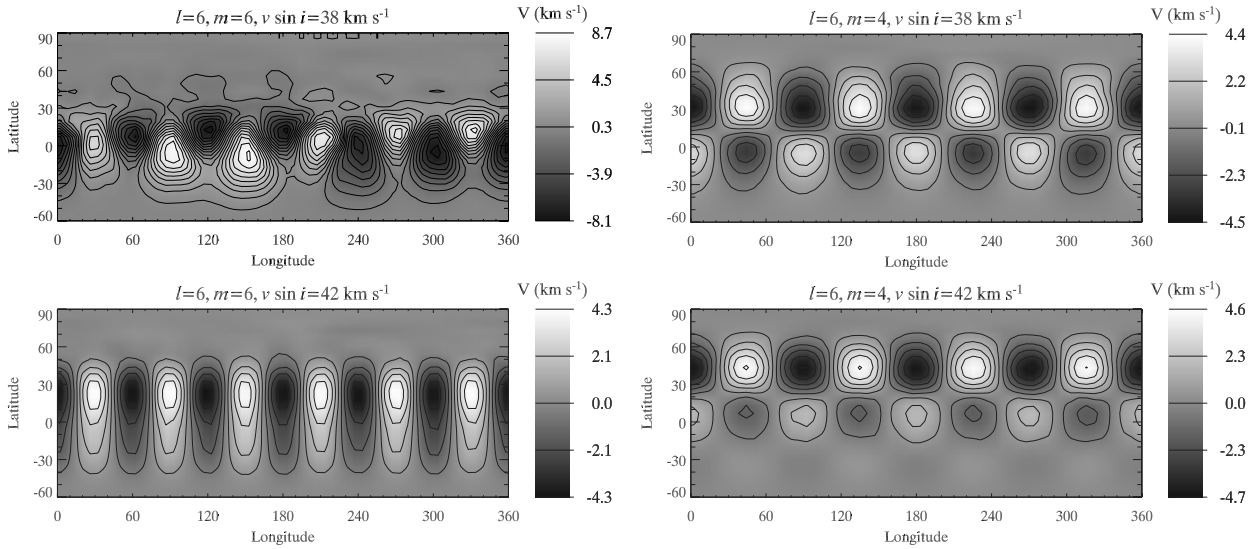

Fig. 13. Influence of errors in the projected rotational velocity on the Doppler reconstruction of the pulsation velocity field. The images show the $V_r^{\rm s}$ velocity map for the $\ell = 6$, $m = 6$, $i = 60^\circ$ (*left panels*) and the $\ell = 6$, $m = 4$, $i = 60^\circ$ (*right panels*) non-radial modes recovered with $v_{\rm e} \sin i$ deviating by ± 2 km s^{-1} from the true value.

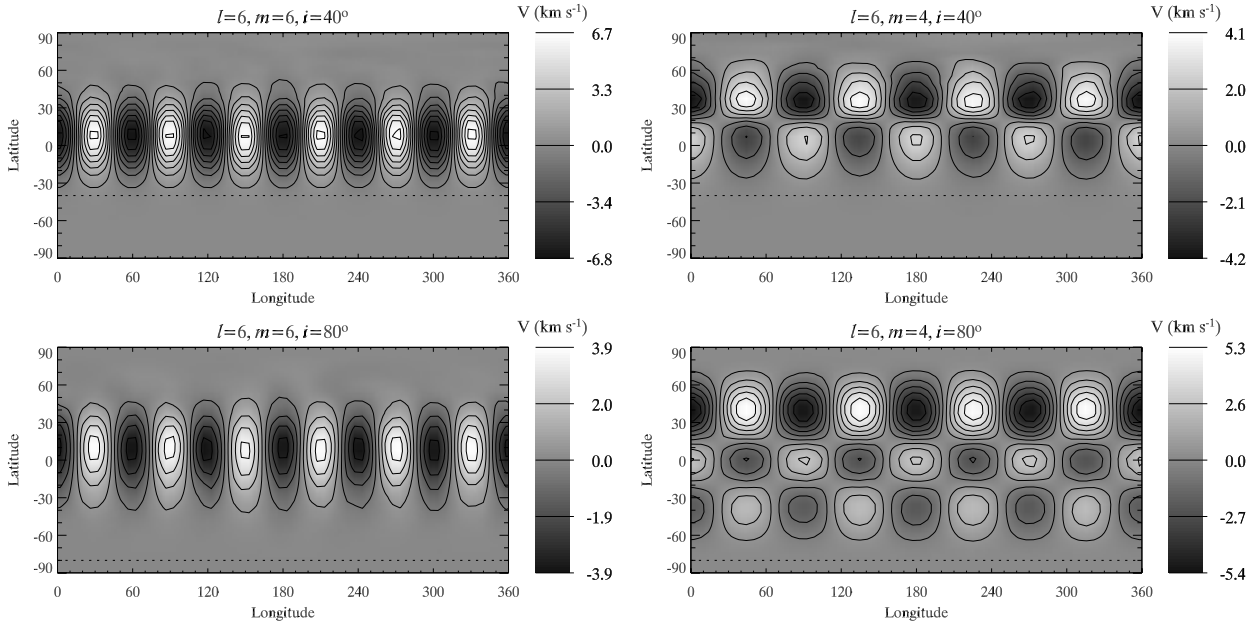

Fig. 14. Influence of errors in the inclination angle on the Doppler reconstruction of the pulsation velocity field. The images show the $V_r^{\rm s}$ velocity map for the $\ell = 6$, $m = 6$, $i = 60^\circ$ (*left panels*) and the $\ell = 6$, $m = 4$, $i = 60^\circ$ (*right panels*) non-radial modes recovered with i deviating by $\pm 20^\circ$ from the true value. These plots show the whole stellar surface and the horizontal dotted line indicates the lowest visible latitude for the inclination angle adopted in the respective velocity field reconstruction.

of the pulsation velocity maps from simulated observational data was performed for a wide range of stellar oscillation geometries, including sectoral, axisymmetric and antisymmetric tesseral, zonal and oblique dipolar non-radial pulsation modes. We show that the velocity inversion technique is successful for *all* the pulsation geometries considered here provided that a non-negligible line profile changes are observed. The only situation encountered in our numerical tests which is characterized by very weak changes in the line profiles and where, consequently, no useful information can be recovered by our code (and by any other spectroscopic technique) is represented by the antisymmetric zonal oscillations observed at high inclination angles.

We investigated the influence of incorrect assumptions about the inclination of the rotation axis i and the projected rotational velocity $v_{\rm e} \sin i$. Deviation of the first parameter by as much as $\pm 20^\circ$ with respect to the true value of the inclination angle has only a weak influence on the recovered surface pulsation velocity structure. In contrast, a moderate and occasionally significant distortion of the pulsation pattern is detected in the

velocity maps recovered with wrong $v_e \sin i$ values. However, in these tests the code was unable to derive a spurious surface image which would provide an adequate fit to the input spectra. Notably, $v_e \sin i$ errors in the surface velocity mapping cannot be partially compensated by invoking a fictitious rotationally symmetric distribution of a surface parameter as in the Doppler mapping of temperature or chemical composition.

We conclude that the pulsation Doppler mapping is generally a robust and reliable technique and has a strong potential to play a primary role in revealing the surface pulsation geometries in many types of pulsating stars across the H-R diagram. The first application of the velocity mapping technique will be presented in a subsequent paper dealing with the oblique non-radial pulsations of the roAp star HR 3831.

Acknowledgements. I am grateful to Professor Nikolai Piskunov for many enlightening discussions of various aspects of the art of Doppler imaging.
This work was supported by the Lise Meitner fellowship granted by the Austrian Science Fund (FWF, project No. M757-N02).

References

Aerts, C., De Pauw, M., & Waelkens, C. 1992, A&A, 266, 294
Aerts, C., & Waelkens, C. 1993, A&A, 273, 135
Aerts, C., & Eyer L. 2000, in Delta Scuti and Related Stars, ed. M. Breger, & M. Montgomery, ASP Conf. Ser., 210, 113
Baade, D., & Weiss, W. W. 1987, A&AS, 67, 147
Balona, L. A. 2000, in Delta Scuti and Related Stars, ed. M. Breger, & M. Montgomery, ASP Conf. Ser., 210, 170
Balona, L. A. 2002, MNRAS, 337, 1059
Berdyugina, S. V., Telting, J. H., & Korhonen, H. 2003, A&A, 406, 273 (BTK)
Bigot, L., & Dziembowski, W. A. 2002, A&A, 391, 235
Brown, S. F., Donati, J.-F., Rees, D. E., & Semel M. 1991, A&A, 250, 463
De Ridder, J., Dupret, M.-A., Neuforge, C., & Aerts, C. 2002, A&A, 385, 572
Gies, D. R., & Kullavanijaya, A. 1988, ApJ, 326, 813
Goncharskii, A. V., Stepanov, V. V., Khokhlova, V. L., & Yagola, A. G. 1977, SvA Lett., 3, 147
Hao, J. 1998, ApJ, 500, 440
Kennelly, E. J., Walker, G. A. H., & Merryfield, W. J. 1992, ApJ, 400, L71
Kochukhov, O., & Ryabchikova, T. 2001, A&A, 374, 615
Kochukhov, O., & Piskunov, N. 2002, A&A, 388, 868
Kurtz, D. W. 1982, MNRAS, 200, 807
Kurucz, R. 1993, CD-ROM No. 13, Smithsonian Astrophys. Obs.
Lee, U., & Saio, H. 1990, ApJ, 349, 570
Lüftinger, T., Kuschnig, R., Piskunov, N. E., & Weiss, W. W. 2003, A&A, 406, 1033
Martens, L., & Smeyers, P. 1982, A&A, 106, 317
Pesnell, W. D. 1990, ApJ, 339, 1038
Piskunov, N. E. 1990, Mem. Soc. Astron. It., 61, 577
Piskunov, N. 1992, in Stellar Magnetism, ed. Yu. V. Glagolevskij, & I. I. Romanyuk (Nauka: St. Petersburg), 92
Piskunov, N., & Kochukhov, O. 2002, A&A, 381, 736
Saio, H., & Gaustchy, A. 2004, MNRAS, 350, 485
Schrijvers, C., Telting, J. H., Aerts, C., Ruymaekers, E., & Henrichs, H. F. 1997, A&AS, 121, 343
Shibahashi, H., & Takata, M. 1993, PASJ, 45, 617
Smeyers, P., & Tassoul, M. 1987, ApJS, 65, 429
Smith, M. A. 1977, ApJ, 215, 574
Socas-Navarro, H., Trujillo Bueno, J., & Ruiz Cobo 2000, ApJ, 530, 977
Strassmeier, K. G., Rice, J. B., Wehlau, W. H., et al. 1991, A&A, 247, 130
Telting, J. 2003, in Asteroseismology Across the HR Diagram, ed. M. J. Thompson, M. S. Cunha, & M. J. P. F. G. Monteiro, Astrophys. Space Sci. Lib., 284, 85
Tikhonov, A. N. 1963, Sov. Math. Dokl., 4, 1624
Vogt, S. S., & Penrod, G. D. 1983, ApJ, 275, 661
Vogt, S. S., Penrod, G. D., & Hatzes, A. P. 1987, ApJ, 321, 496